Inorganic Chemistry

Article

pubs.acs.org/IC

Control in the Rate-Determining Step Provides a Promising Strategy To Develop New Catalysts for CO_2 Hydrogenation: A Local Pair Natural Orbital Coupled Cluster Theory Study

Bhaskar Mondal, Frank Neese, and Shengfa Ye*

Department of Molecular Theory and Spectroscopy, Max-Planck Institute for Chemical Energy Conversion, Stiftstrasse 34-36, D-45470 Mülheim an der Ruhr, Germany

Supporting Information

ABSTRACT: The development of efficient catalysts with base metals for CO_2 hydrogenation has always been a major thrust of interest. A series of experimental and theoretical work has revealed that the catalytic cycle typically involves two key steps, namely, base-promoted heterolytic H_2 splitting and hydride transfer to CO_2, either of which can be the rate-determining step (RDS) of the entire reaction. To explore the determining factor for the nature of RDS, we present herein a comparative mechanistic investigation on CO_2 hydrogenation mediated by $[M(H)(\eta^2\text{-}H_2)(PP_3^{Ph})]^{n+}$ (M = Fe(II), Ru(II), and Co(III); PP_3^{Ph} = tris(2-(diphenylphosphino)phenyl)phosphine) type complexes. In order to construct reliable free energy profiles, we used highly correlated wave function based ab initio methods of the coupled cluster type alongside the standard density functional theory. Our calculations demonstrate that the hydricity of the metal−hydride intermediate generated by H_2 splitting dictates the nature of the RDS for the Fe(II) and Co(III) systems, while the RDS for the Ru(II) catalyst appears to be ambiguous. CO_2 hydrogenation catalyzed by the Fe(II) complex that possesses moderate hydricity traverses an H_2-splitting RDS, whereas the RDS for the high-hydricity Co(III) species is found to be the hydride transfer. Thus, our findings suggest that hydricity can be used as a practical guide in future catalyst design. Enhancing the electron-accepting ability of low-hydricity catalysts is likely to improve their catalytic performance, while increasing the electron-donating ability of high-hydricity complexes may speed up CO_2 conversion. Moreover, we also established the active roles of base NEt_3 in directing the heterolytic H_2 splitting and assisting product release through the formation of an acid−base complex.

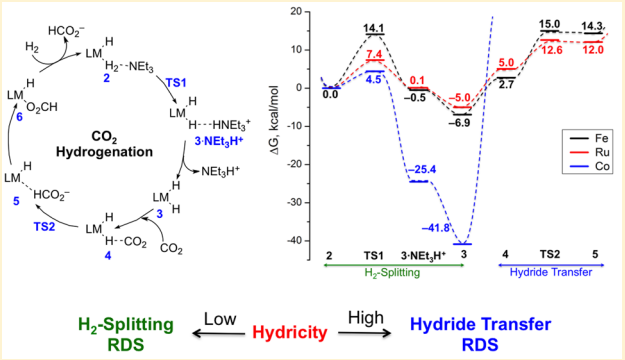

INTRODUCTION

Research related to CO_2 activation has been intensified in recent years due to the persistently rising level of CO_2, a major greenhouse gas in the atmosphere that contributes to global warming.[1] On the other hand, CO_2 is an abundant and nontoxic C1 source that can be used in the synthesis of liquid fuels and fine chemicals.[2] Catalytic CO_2 hydrogenation to formic acid and its derivatives has been shown to be a promising way to transform CO_2 into useful chemical feedstock.[3] To date, catalysts based on precious metals such as rhodium,[4] ruthenium,[5] and iridium[6] have been extensively employed for CO_2 functionalization. However, reactions using base metal catalysts like iron, nickel, or cobalt are still under development, presumably because of the low reactivity. Recently, pioneering work reported that several 3d metal catalysts can show similar activity to noble metals.[7] However, the harsh conditions (high temperature, high pressure, and strong base) that have to be employed limit the large-scale application. A deep understanding of the reaction mechanism at the atomic level is therefore highly desired. To this end, we investigate the reactivity of three complexes of the type $[M(H)(\eta^2\text{-}H_2)(PP_3^{Ph})]^{n+}$ (M = Fe(II) ($\mathbf{1}_{Fe}$), Ru(II) ($\mathbf{1}_{Ru}$), and Co(III) ($\mathbf{1}_{Co}$)) toward CO_2 conversion to provide invaluable insights into the nature of the RDS. It should be pointed out that complex $\mathbf{1}_{Fe}$ has already been reported to be an efficient catalyst for CO_2 hydrogenation.[7b]

Experimental work has concluded that $\mathbf{1}_{Fe}$ itself is catalytically inactive because no formic acid or formate can be formed when $\mathbf{1}_{Fe}$ is exposed to CO_2.[7b] Addition of NEt_3 initiates the reaction. However, no intermediates have been detected yet in the subsequent reaction. Hence, formation of a dihydride intermediate $[Fe^{II}(H)_2(PP_3^{Ph})]$ ($\mathbf{3}_{Fe}$) via base-promoted heterolytic H_2 splitting ($\mathbf{2} \rightarrow \mathbf{3}\cdot NEt_3H^+$, Scheme 1) was proposed, and $\mathbf{3}_{Fe}$ is considered to be the active form of the catalyst. Complex $\mathbf{3}_{Fe}$ performs hydride transfer ($\mathbf{4} \rightarrow \mathbf{5}$) to CO_2 to give $\mathbf{5}_{Fe}$, which then undergoes formate rebound ($\mathbf{5} \rightarrow \mathbf{6}$) to yield a metal−formate complex ($\mathbf{6}_{Fe}$). Finally, regeneration of catalyst $\mathbf{1}$ is accomplished via ligand exchange between H_2 and formate ($\mathbf{6} \rightarrow \mathbf{1}$).

Received: February 27, 2015
Published: July 23, 2015

DOI: 10.1021/acs.inorgchem.5b00469
Inorg. Chem. 2015, 54, 7192−7198

Scheme 1. Proposed Catalytic Pathway

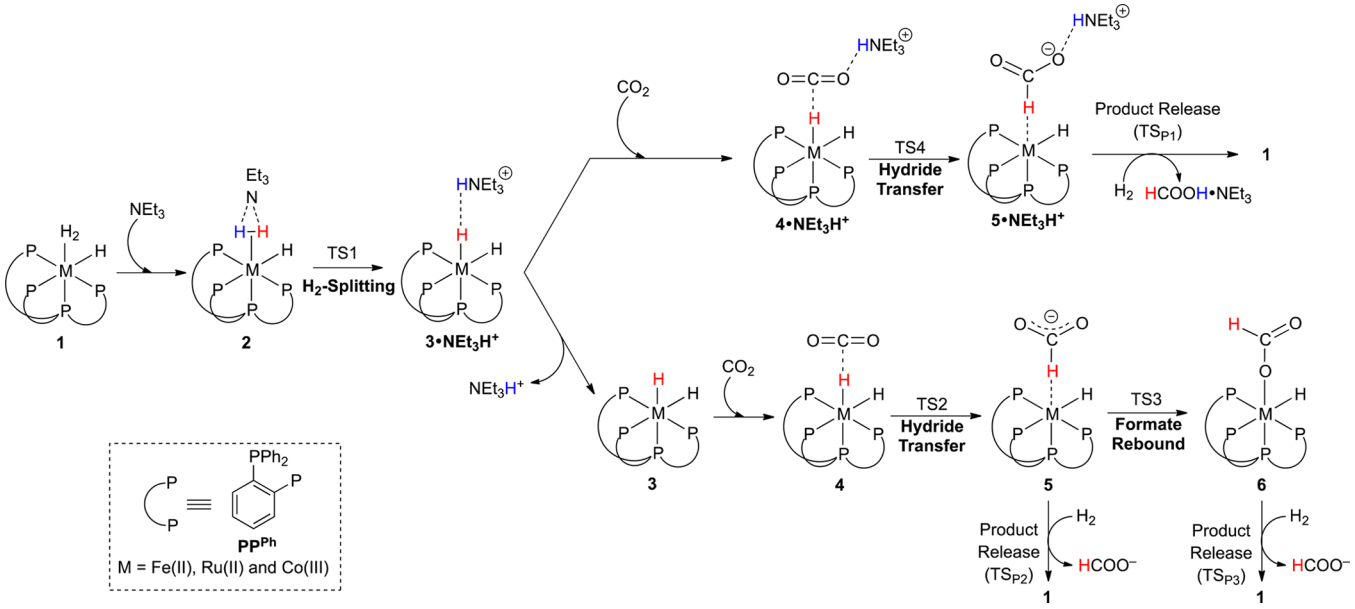

Among the elementary reaction steps described in Scheme 1, the base-promoted heterolytic H_2 splitting and hydride transfer to CO_2 are the two crucial steps in CO_2 hydrogenation as found for the reactions with Fe-,[7a] Ru-,[8] Rh-,[8c,9] and Ir-based[10] catalysts. Theoretical studies on closely related systems $[(PNP)Ir^{III}(H)_3]$, $[(PNP)Co^{III}(H)_3]$, and $[(PNP)Fe^{II}(H)_2(CO)]$ (PNP = 2,6-bis(dialkylphosphinomethyl)-pyridine)[11] showed that H_2 splitting is the RDS. The same holds true for half-sandwich complexes $[Cp^*M^{III}(6,6'\text{-}O^-\text{-}bpy)(H_2O)]$ (M = Co, Rh, and Ir; bpy = 2,2′-bipyridine).[12] However, CO_2 conversion mediated by $[(\eta^5\text{-}C_5Me_5)Ir^{III}(bpy)(H)]^+$ was dissected experimentally to traverse a hydride transfer RDS, while for its Ru(II) analogue, $[(\eta^6\text{-}C_6Me_6)Ru^{II}(bpy)(H)]^+$, the RDS was identified to be H_2 splitting.[13] Additionally, the recent experimental study on the $[Co^I(dmpe)_2H]$ (dmpe = 1,2-bis(dimethylphosphino)ethane) has suggested the hydride transfer to be the RDS in the presence of a strong base.[14] Evidently, identifying and understanding the nature of the RDS is pivotal for improvement of the activity of available catalysts and for future design of new systems. This raises an interesting question about what factor determines the chemistry of the RDS. However, to our knowledge no systematic investigation aiming at addressing this question has been reported yet, since most computational work has been dedicated to elucidating the reaction mechanisms of individual systems involving different metal centers and supporting ligands.[10,11,15] In the present contribution, we carried out a theoretical study on CO_2 hydrogenation catalyzed by $\mathbf{1}_{Fe}$ along with its hypothetical Ru(II) ($\mathbf{1}_{Ru}$) and Co(III) ($\mathbf{1}_{Co}$) congeners in order to shed light on this question. The three complexes are isoelectronic and besides Fe, Ru, and Co have also been found to be the metal centers in the range of efficient catalysts toward CO_2 utilization (vide supra).[1b]

Given the limited accuracy that density functional theory (DFT) methods can achieve in predicting reaction energetics involving transition metals,[16] we employed highly correlated wave function-based ab initio method of the coupled cluster (CC)[17] type in this study to calculate more reliable reaction energetics with chemical accuracy (<3 kcal/mol).[18] Notably, the size of the species under consideration is certainly beyond the reach of the canonical CC method. Fortunately, due to recent developments it is possible to perform such CC calculations with affordable computational cost. Specifically, the domain-based local pair natural orbital coupled cluster approach with single and double excitations and perturbative triples corrections (DLPNO-CCSD(T))[19] has been used to compute critical points on the relevant potential energy surfaces, for which DLPNO-CCSD(T) calculations with more than 3100 basis functions have been undertaken. Our earlier studies[20] demonstrated the robustness and accuracy of this method and showed that its computational cost is only about 5 times higher than that for the conventional hybrid DFT calculations (Table S1, Supporting Information).

■ COMPUTATIONAL SETUP

All calculations were performed with the ORCA program package.[21] The geometries were optimized using the meta-GGA (GGA = generalized gradient approximation) M06-L[22] density functional in conjunction with the scalar relativistic zeroth-order regular approximation (ZORA).[23] The Ahlrichs triple-ζ quality basis set without *f*-polarization functions, def2-TZVP(-*f*),[24] was used for Fe, P, N, H, H_2, and CO_2, and the rest of the atoms were described with double-ζ quality split-valence basis set, def2-SVP.[23b] We selected M06-L because it has been reported that this functional is able to account for noncovalent interactions accurately.[25] For comparison, we also optimized the geometries using the pure-GGA BP86 density functional[26] in conjunction with atom-pairwise dispersion corrections with Becke–Johnson damping (D3BJ)[27] to treat the noncovalent interactions. A detailed discussion on the performance of the M06-L functional over BP86 is documented in the Supporting Information. For all geometry optimizations, we used a convergence tolerance of 5×10^{-6} E_h for energy changes, 3×10^{-4} E_h/bohr for maximum gradients, 1×10^{-4} E_h/bohr for root-mean-square (RMS) gradients, 4×10^{-3} bohr for maximum displacements, and 2×10^{-3} bohr for RMS displacements. The numerical integration grid level 5 (Grid5) was used for the DFT computations. Tight convergence criteria (energy tolerance 1×10^{-8} E_h) for self-consistent field (SCF) calculations were employed throughout the DFT computations.

The density fitting approximation (or the resolution of the identity approximation (RI-J)) was used to accelerate the evaluation of the Coulomb terms in density functional calculations with a negligible loss in "chemical accuracy" (~1 mE_h).[28] The utilization of the RI-J

DOI: 10.1021/acs.inorgchem.5b00469
Inorg. Chem. 2015, 54, 7192−7198

approximation requires an auxiliary Coulomb-fitting basis set, which was provided by the Ahlrichs Coulomb-fitting basis set, def2-TZV/J[28b,29] for our calculations. The conductor-like screening solvation model (COSMO)[30] was applied with solvent methanol (ε = 32.63) during the geometry optimizations and single-point energy calculations at the DFT level. To be consistent with experiment, methanol was selected as the solvent.[7b] The geometry optimizations were performed without any constraints. The subsequent numerical harmonic frequency calculations revealed that local minima have all real frequencies, and transition states (TSs) have a single imaginary frequency. The connectivity of each TS has been validated through a relaxed potential energy surface scan for the corresponding reaction coordinate, and the TS was found to be the highest-energy point that connects the relevant reactant and product (Figures S3−S5, Supporting Information). The zero-point vibrational energies, thermal corrections, and entropy terms for all structures were obtained from the harmonic frequency calculations at the M06-L level. A list of these corrections for all reaction species is tabulated in Table S2, Supporting Information.

Final single-point energy calculations were performed at two different levels of density functional theories, namely, M06-L and B3LYP (a hybrid density functional with 20% Hartree−Fock (HF) exchange)[31] in conjunction with the more flexible def2-TZVPP[32] (includes high angular momentum polarization functions for all elements) basis set for all atoms. For hybrid DFT computations, the calculation of the HF exchange terms usually dominates the overall executing time. This problem can be resolved by the "chain of spheres" COSX[33] approximation. A combination of this treatment for the HF exchange term along with the RI-J approximation for the Coulomb term was invoked for the hybrid DFT calculations with the ORCA keyword RIJCOSX (a description of the input file is provided in the Supporting Information). This calculation also requires an auxiliary Coulomb fitting basis set, which was provided by def2-TZVPP/J[28a] for our calculations. The hybrid DFT-level single-point energy calculations were also performed in conjunction with the D3BJ dispersion corrections.

Finally, highly accurate electronic energies were computed using DLPNO-CCSD(T) in conjunction with the def2-TZVPP basis set. Our earlier work shows CCSD calculations with the def2-TZVPP basis set yield accurate electronic energies close to those with the complete basis set limit.[34] The correlation fitting auxiliary basis set def2-TZVPP/C was used to accelerate the DLPNO-CCSD(T) calculations. The RIJCOSX approximation was also applied during DLPNO-CCSD(T) calculations with the auxiliary Coulomb fitting basis set def2-TZVPP/J. Here the RIJCOSX approximation treats expensive integral transformations in the DLPNO part along with the initial SCF calculations. Solvent corrections (Table S2, Supporting Information) to CC electronic energies were obtained from the M06-L single-point energy calculations.

For association reactions such as substrate binding, calculations using the infinitely separated reactants as the reference typically predict a substantial entropy increase of about 10−15 kcal/mol. This is due to the loss in translational and rotational degrees of freedom of reactant complexes in the gas phase. However, for reactions occurring in solution, this approximation is expected to cause a considerable error in the estimated entropy. Due to the fact that only when all reactants enter into the same solvent cage can the reaction readily take place, for each individual reactant the vast majority of translational and rotational degrees of freedom have thus been suppressed by interactions between different reactants and between reactants and solvent molecules. In line with this analysis, our earlier work shows that this approximation leads to a constant error of about 13 kcal/mol in the computed entropy.[35] In fact, one can safely assume that a series of pre-equilibriums between different reactants have been set up before the actual reaction happens.[36] Therefore, it is more reliable to calculate intrinsic reaction barriers with reference to reactant complexes, although such a treatment may marginally underestimate the entropy change.

RESULTS AND DISCUSSION

Complexes $\mathbf{1}_{Fe}$, $\mathbf{1}_{Ru}$, and $\mathbf{1}_{Co}$ are computationally predicted to possess a low-spin singlet ground state with an intermediate-spin triplet state lying 39.5, 60.0, and 26.7 kcal/mol higher in energy, respectively (M06-L/def2-TZVPP value). The geometry optimization of the corresponding high-spin quintet states leads to dissociation of the η^2-H_2 ligand from the metal center. Additionally, the singlet−triplet gap of 35.4 kcal/mol for $\mathbf{1}_{Fe}$ estimated by the B3LYP functional is close to the M06-L value and appears to be independent of the level of theory used. Clearly, the computed energy gaps are much larger than the activation barriers of the RDSs (vide infra) even considering the large error range of DFT calculations in predicting spin-state energetics for transition metal complexes.[37] Hence, the possibility of multistate reactivity can be safely ruled out, and the reaction energetics is therefore probed on the singlet free energy profiles only.

Figure 1 presents the reaction free energy profile calculated at the DLPNO-CCSD(T) level for the proposed catalytic cycle

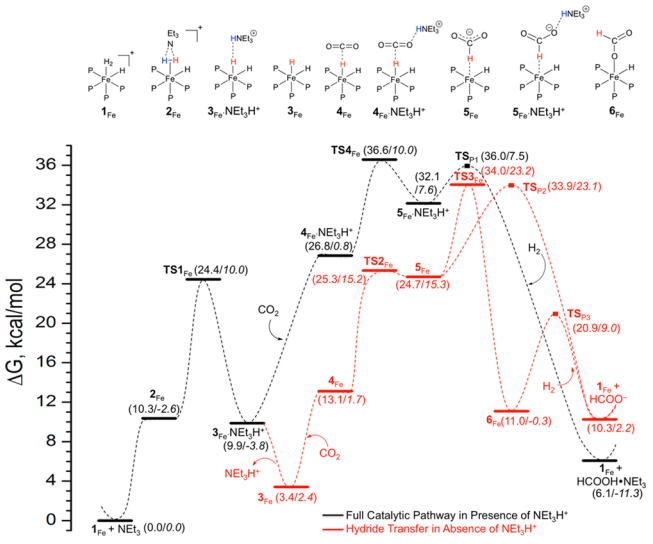

Figure 1. DLPNO-CCSD(T)/def2-TZVPP Gibbs free energy (ΔG) profile for the full catalytic cycle of CO_2 hydrogenation by $\mathbf{1}_{Fe}$. Enthalpy changes (ΔH) are given in italics along with ΔG. Transition states TS_{P1}, TS_{P2}, and TS_{P3} could not be located properly.

of $\mathbf{1}_{Fe}$ as shown in Scheme 1. First, our theoretical results confirm the inertness of $\mathbf{1}_{Fe}$ toward CO_2 hydrogenation observed experimentally (Figure S6, Supporting Information). The first part of the reaction is base-promoted heterolytic H_2 splitting ($\mathbf{1}_{Fe} \rightarrow \mathbf{3}_{Fe}$) to generate catalytically active dihydride species ($\mathbf{3}_{Fe}$) with an intrinsic barrier of 14.1 kcal/mol. The elementary H_2-splitting step ($\mathbf{2}_{Fe} \rightarrow \mathbf{3}_{Fe}\cdot NEt_3H^+$) is nearly thermoneutral. The release of the conjugate acid NEt_3H^+ results in an increase in the entropy, making the whole process ($\mathbf{1}_{Fe} + NEt_3 \rightarrow \mathbf{3}_{Fe} + NEt_3H^+$) slightly endergonic by 3.4 kcal/mol. We considered the next hydride transfer step in the presence ($\mathbf{4}_{Fe}\cdot NEt_3H^+ \rightarrow \mathbf{5}_{Fe}\cdot NEt_3H^+$ via $\mathbf{TS4}_{Fe}$) or absence ($\mathbf{4}_{Fe} \rightarrow \mathbf{5}_{Fe}$ via $\mathbf{TS2}_{Fe}$) of the conjugate acid NEt_3H^+. An appreciable effect of NEt_3H^+ on the reaction free energies has been observed. The reaction with $\mathbf{4}_{Fe}$ is highly endergonic (11.6 kcal/mol), whereas binding of NEt_3H^+ to $\mathbf{4}_{Fe}$ substantially lowers the reaction endergonicity by 6.3 kcal/mol. As a consequence, the hydride transfer barrier for $\mathbf{4}_{Fe}\cdot NEt_3H^+$ (9.8 kcal/mol) is lower than that for $\mathbf{4}_{Fe}$ (12.2 kcal/mol). The

DOI: 10.1021/acs.inorgchem.5b00469
Inorg. Chem. 2015, 54, 7192−7198

consecutive formate rebound step ($\mathbf{5}_{Fe} \rightarrow \mathbf{6}_{Fe}$) is significantly exergonic by 13.6 kcal/mol due to the formation of a stable metal−formate complex, $\mathbf{6}_{Fe}$, and is associated with an intrinsic reaction barrier of 9.3 kcal/mol ($\mathbf{TS3}_{Fe}$), in agreement with the value (8 kcal/mol) reported for $[(PNP)Ir^{III}(H)_3]$.[11a] However, the formate release from $\mathbf{6}_{Fe}$ is rather energetically costly due to the strong Fe−$^{-}$OC(O)H bonding interaction. The relaxed potential energy surface scan along the Fe−O bond length shows that the reaction energy constantly rises up, because this process would presumably yield a coordinatively unsaturated complex (Figure S10, Supporting Information). Moreover, the energetic penalty exceeds 20 kcal/mol at a Fe−O distance of 2.9 Å, beyond which a new Fe−O bond forms between the iron center and the other oxygen atom of the being dissociated formate. We thus considered two other separate routes for product dissociation and catalyst regeneration through H_2 binding, from $\mathbf{5}_{Fe}{\cdot}NEt_3H^+$ and $\mathbf{5}_{Fe}$. Remarkably, the rise in energy for $\mathbf{6}_{Fe}$ is much steeper than those found for $\mathbf{5}_{Fe}$ and $\mathbf{5}_{Fe}{\cdot}NEt_3H^+$ (Figure S9, Supporting Information), clearly indicating that $\mathbf{5}_{Fe}$ and $\mathbf{5}_{Fe}{\cdot}NEt_3H^+$ releases the product more easily than $\mathbf{6}_{Fe}$ does. Due to the formation of an acid−base complex ($HCOOH{\cdot}NEt_3$) the product release from $\mathbf{5}_{Fe}{\cdot}NEt_3H^+$ is even more favored compared to $\mathbf{5}_{Fe}$. Although we could not locate the corresponding transition states, a rough estimate of the barriers for the three product dissociation channels can be achieved on the basis of the relaxed surface scans presented in Figures S9 and 10, Supporting Information. For the direct product release from $\mathbf{5}_{Fe}{\cdot}NEt_3H^+$ ($\mathbf{TS}_{P1}$) and $\mathbf{5}_{Fe}$ ($\mathbf{TS}_{P2}$) (Figure 1), the Fe−H distance is constrained at 2.5 Å, similar to the actual Fe−H distance observed in the formate-rebound TS ($\mathbf{TS3}_{Fe}$, Fe−H = 2.541 Å). For comparison, in the case of the formate dissociation from $\mathbf{6}_{Fe}$, the TS ($\mathbf{TS}_{P3}$) (Figure 1) is obtained by fixing the Fe−O distance at 2.5 Å. This may significantly underestimate the barrier via $\mathbf{TS}_{P3}$ because of the different radii of H and O atoms; nevertheless, we can estimate the barrier approximately. Of the three pathways, the product release from $\mathbf{5}_{Fe}{\cdot}NEt_3H^+$ encounters the highest driving force (26 kcal/mol) and hence the lowest barrier (~4 kcal/mol), thereby highlighting the role of the conjugate acid (NEt_3H^+) in speeding up the product release (The corresponding enthalpy changes (ΔH) for the product release are presented in Scheme S1, Supporting Information). Taken together, a concerted process of the formate dissociation from $\mathbf{5}_{Fe}{\cdot}NEt_3H^+$ ($\mathbf{5}_{Fe}{\cdot}NEt_3H^+ \rightarrow \mathbf{1}_{Fe} + HCOOH{\cdot}NEt_3$) and H_2 association is most likely to occur, consistent with that found for $[(PNP)Ir^{III}(H)_3]$.[11a]

Considering the intrinsic reaction barriers in Figures 1 and S7, Supporting Information, both CCSD(T) and DFT-M06-L calculations unanimously predict the base-promoted heterolytic splitting is the RDS of the CO_2 hydrogenation by $\mathbf{1}_{Fe}$. The CCSD(T)-computed barrier of the RDS step is 14.1 kcal/mol, which translates to 14.5 kcal/mol at the actual experimental temperature (100 °C). This value is lower than the activation free energy of ~25 kcal/mol (at 100 °C and 60 bar) deduced from the experimental turnover frequency (TOF) of 85 h^{-1}.[7b] The discrepancy can largely be attributed to the underestimation of the entropic contribution arising from calculating the barrier with respect to the reactant complex ($\mathbf{2}_{Fe}$). On the other hand, the estimated reaction barrier (24.4 kcal/mol) using the infinitely separated reactants ($\mathbf{1}_{Fe}$ + NEt_3) as the reference is in close agreement with the experiment despite the fact that such calculations overestimate entropic contributions. Thus, a direct comparison of the calculated barrier to the experimental data requires more caution. However, the relative barriers for different steps should be much more reliable due to error cancellation. In comparison with the CCSD(T) results, both M06-L and B3LYP calculations further underestimate the intrinsic reaction barriers by 4 kcal/mol (Figure S8, Supporting Information), which lends credence to the accuracy of the DLPNO-CCSD(T) approach.

As we intend to explore the determining factor for the RDSs of the CO_2 hydrogenation, the following discussion is therefore focused on the heterolytic H_2 splitting and the hydride transfer ($\mathbf{2} \rightarrow \mathbf{3}$ via $\mathbf{TS1}$ and $\mathbf{4} \rightarrow \mathbf{5}$ via $\mathbf{TS2}$). The free energy profiles for $\mathbf{1}_{Fe}$, $\mathbf{1}_{Ru}$, and $\mathbf{1}_{Co}$ shown in Figure 2 only consist of the key

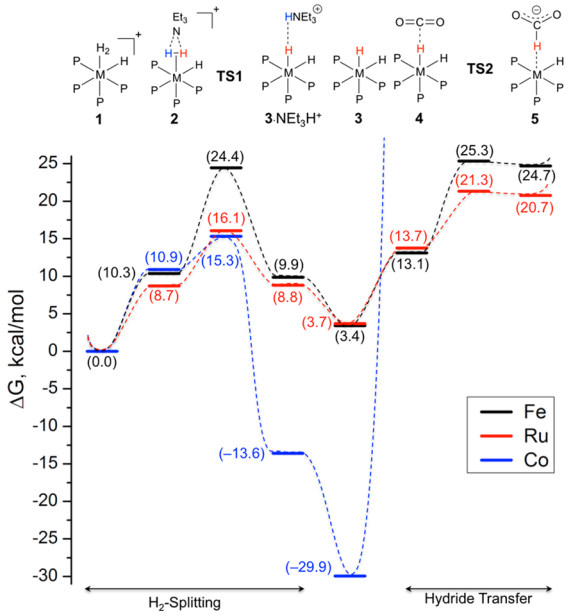

Figure 2. Gibbs free energy (ΔG) profiles for the key steps of CO_2 hydrogenation at the DLPNO-CCSD(T)/def2-TZVPP level of theory.

steps. For both steps, overall the computed Gibbs free energy profiles using DFT and DLPNO-CCSD(T)/def2-TZVPP are qualitatively parallel, albeit with the largest barrier difference of ~9 kcal/mol. The DFT free energy profiles at the M06-L and B3LYP levels are also presented in Figure S8, Supporting Information. We found that the considerable difference between the DLPNO-CCSD(T) and the DFT energy profiles occurs at the steps of the formation of the reactant complex ($\mathbf{1}$ + $NEt_3 \rightarrow \mathbf{2}$), of the release of NEt_3H^+ ($\mathbf{3}{\cdot}NEt_3H^+ \rightarrow \mathbf{3}$ + NEt_3H^+), and of the hydride transfer ($\mathbf{4} \rightarrow \mathbf{5}$) (for a detailed discussion see the Supporting Information). Despite the above quantitative differences, the calculations at both levels of theory unanimously predict the same RDS for the CO_2 hydrogenation by the three systems under investigation. For $\mathbf{1}_{Fe}$, the heterolytic H_2 splitting is calculated to be RDS, whereas the hydride transfer process is difficult to occur for $\mathbf{1}_{Co}$. The hydride transfer from $\mathbf{3}_{Co}$ to CO_2 was carefully probed by a relaxed surface scan at a series of $Co^{III}H{\cdots}CO_2$ separations, and the results reveal that CO_2 successively approaching the hydride causes a monotonic increase in energy (Figure S11, Supporting Information). At a C−H distance of 1.10 Å, the bond length close to formate ($HCOO^-$), the CO_2 adduct is found to be unstable by more than 20 kcal/mol relative to $\mathbf{3}_{Co}$ and CO_2. A similar situation is also found in the presence of NEt_3H^+. Therefore, even if CO_2 hydrogenation with $\mathbf{1}_{Co}$ could

DOI: 10.1021/acs.inorgchem.5b00469
Inorg. Chem. 2015, 54, 7192−7198

take place, the hydride transfer would be the RDS. Taken together, switching the metal center from Fe(II) to Co(III) changes the RDS from H_2 splitting to hydride transfer. In the case of $\mathbf{1}_{Ru}$, the difference (~2 kcal/mol) in the reaction barriers computed for both steps is close to the limit of the DLPNO-CCSD(T) methodology,[19b] and hence, the RDS of the CO_2 hydrogenation by $\mathbf{1}_{Ru}$ cannot be assigned unambiguously. The barriers are lower than those estimated for the RDSs of $\mathbf{1}_{Fe}$ and $\mathbf{1}_{Co}$, which points to a higher reactivity for the Ru(II) complex compared to the Fe(II) and Co(III) complexes.

For the H_2-splitting process, as depicted in Figure 2, the H_2-splitting step is thermoneutral for $\mathbf{1}_{Fe}$ and $\mathbf{1}_{Ru}$, which is highly exergonic for $\mathbf{1}_{Co}$. The reaction energy reflects the stability of metal−dihydrogen complex **2** relative to metal−dihydride species **3**. Specifically, one needs to compare the differential bond strength between M−H_2 and M−H^-, as NEt_3H^+ is a common product of the reaction. The binding enthalpies of η^2-H_2 with $\mathbf{1}_{Fe}$, $\mathbf{1}_{Ru}$, and $\mathbf{1}_{Co}$ calculated by DLPNO-CCSD(T) are −36.9, −30.6, and −35.2 kcal/mol, respectively (Table 1).

Table 1. η^2-H_2 Binding Parameters for Three Complexes

	H1−H2[a]	M−H1[a]	M−H2[a]	q[b] (q_{H1}, q_{H2})	ΔH_B[c]	ΔH_B[d]
$\mathbf{1}_{Fe}$	0.854	1.633	1.614	0.07, 0.10	−33.6	−36.9
$\mathbf{1}_{Ru}$	0.844	1.803	1.784	0.07, 0.10	−28.4	−30.6
$\mathbf{1}_{Co}$	0.842	1.622	1.608	0.08, 0.12	−31.1	−35.2

[a]Bond lengths in Angstroms. [b]Löwdin atomic charges. [c]M06-L-calculated binding enthalpies (ΔH_B, in kcal/mol). [d]DLPNO-CCSD-(T)values for ΔH_B (in kcal/mol).

Thus, the differential M−H_2 interaction is not the key reason for the drastically different reaction energy because the latter spans a range of ~30 kcal/mol. The weaker metal−hydrogen bonding in $\mathbf{1}_{Ru}$ relative to that in $\mathbf{1}_{Fe}$ is consistent with earlier experimental and theoretical studies.[38] As a result, the difference in the driving force must mainly originate from the differential interaction strength of the M−H^- bond in the metal−hydride complex (**3**), which can easily be quantified by its hydricity. Hydricity, $\Delta G^{\circ}_{H-}(MH)$, measures the ability of a metal−hydride complex (MH) to donate its hydride, MH → M^+ + H^-.[39] Obviously, a less positive $\Delta G^{\circ}_{H-}(MH)$ value corresponds to higher hydride-donating ability and lower hydricity. In other words, metal complexes that stabilize the hydride more through a stronger M−H^- bond has lower hydride-donating ability and higher hydricity. The calculated hydricities in acetonitrile are in the following order within the computational uncertainty of ~8 kcal/mol (Figure S12, Supporting Information), $\mathbf{3}_{Ru}$, 58.5 kcal/mol ≤ $\mathbf{3}_{Fe}$, 66.5 kcal/mol ≪ $\mathbf{3}_{Co}$, 100.0 kcal/mol (the M06-L/def2-TZVPP values, the calculation protocol is documented in the Supporting Information). This rationalizes the largest driving force found for the Co(III) complex. The stronger M−H_2 and M−H^- interactions computed for the Fe(II) species than those for the Ru(II) complex may explain their nearly identical reaction energies. As such, the substantially higher hydricity of $\mathbf{3}_{Co}$ makes it a strong hydride acceptor, whereas $\mathbf{3}_{Fe}$ and $\mathbf{3}_{Ru}$ are weaker hydride acceptors due to their moderate hydricity. The barriers of the two 3d-metal catalysts follow the trend of their driving forces,[40] suggesting that the hydricity is the crucial factor that modulates the reaction barrier. Interestingly, the reactivity of $\mathbf{3}_{Ru}$ does not comply with the Bell−Evan−Polanyi principle.[40b] A systematic study aiming to clarify the effect of the distinct bonding[41] between 3d−1s and 4d−1s on the reactivity of H_2 splitting will be reported in a subsequent publication.

As reported earlier,[7c,42] the reactivity of a metal−hydride complex toward hydride transfer can be elegantly correlated with its hydricity. In the present case, the highest hydricity of $\mathbf{3}_{Co}$ blocks the further reaction. On the contrary, $\mathbf{3}_{Fe}$ and $\mathbf{3}_{Ru}$ with much lower hydricities involve low reaction barriers for the hydride transfer stage. The lower hydricity of $\mathbf{3}_{Ru}$ renders this process more facile, in agreement with the trend reported by relevant experimental studies, for instance, the higher hydride-transfer reactivity observed for $Cp^*(CO)_2RuH$ relative to its iron congener.[43] The calculated reaction energies for the hydride transfer and product release by $\mathbf{3}_{Ru}$ and $\mathbf{3}_{Fe}$ are close to zero, consistent with the observation that hydride transfer is typically an equilibrium reaction.[44] However, formation of a stable acid−base complex, such as $HCOOH{\cdot}NEt_3$ in the present case, should drive the reaction forward due to the significantly elevated driving force (vide supra). Although $\mathbf{3}_{Fe}$, $\mathbf{3}_{Ru}$, and $\mathbf{3}_{Co}$ have the same number of d electrons, the higher hydricity of $\mathbf{3}_{Co}$ can be traced back to the higher oxidation state of the metal center and hence the higher total charge of the complex. Therefore, cobalt complexes with low-valent metal centers are likely to be promising catalysts for CO_2 hydrogenation. In fact, phosphine-based Co(I) hydride complexes have shown impressive catalytic activity under ambient conditions.[7c,45] On the other hand, Co(III) centers coordinated by charge-neutralizing anionic ligands are also expected to exhibit high reactivity, as shown by a recently reported Co(III) complex, $[Cp^*Co^{III}(6,6'\text{-}O^-\text{-bpy})(H_2O)]$.[46] In addition to the metal oxidation state, the spin state also influences the hydricity of a metal−hydride complex. As found for $^3\mathbf{1}_{Fe}$, one e_g-derived orbital with respect to the Fe−H^- σ interaction is singly occupied, which substantially weakens the bonding between them. In line with this reasoning, low-spin ground states prevail in 3d transition metal−hydride complexes[11,15a,c] as well as in the active site of hydrogenases.[47]

Furthermore, our calculations have established the roles of bases in CO_2 hydrogenation reactions. The base NEt_3 directs H_2 heterolysis rather than homolysis, because the homolytic H_2 splitting in $\mathbf{2}_{Fe}$ increases the endothermicity by ~55 kcal/mol compared to the heterolytic cleavage pathway. In addition, the generated conjugate acid NEt_3H^+ can stabilize complex **4** via hydrogen-bonding interactions with the coordinated CO_2 ligand. In this context, Fujita and co-workers showed that perfectly positioned bases could accelerate the H_2 splitting.[48] Above all, the base escalates the thermodynamic driving force of the entire reaction by forming an acid−base complex, which speeds up product release.[3b,4a] In the current case, the formation of $HCOOH{\cdot}NEt_3$ drives the reaction more exergonic by ~11 kcal/mol than the case where the base is absent (Figure 1). Thus, NEt_3 plays a dual role here: one is to promote the heterolytic H_2 splitting, and the other is to assist product release through formation of the acid−base complex.

CONCLUSION

In conclusion, our calculations using the highly correlated DLPNO-CCSD(T) approach reveal that the hydricity of a metal−hydride complex controls the nature and barrier of the RDS. The reactions with the Fe(II) complexes possessing low hydricity pass through an H_2-splitting RDS, whereas for the Co(III) species having much higher hydricity, hydride transfer is found to be rate limiting. Thus, one can classify metal

DOI: 10.1021/acs.inorgchem.5b00469
Inorg. Chem. 2015, 54, 7192−7198

catalysts for CO_2 hydrogenation into two different categories based on their hydricity. For low-hydricity catalysts, adding electron-withdrawing groups in the supporting ligand should accelerate the reaction, while for high-hydricity catalysts, one needs to enhance the electron-donating ability of the system. Thus, we provide a valuable strategy to design new catalysts with higher efficiency. A systematic study along this route is in progress. The present investigation also demonstrates that a delicate balance between the barriers for the two critical reaction steps can be achieved, as demonstrated by $\mathbf{1}_{Ru}$. The dual role of the base in promoting both H_2 heterolysis and formate release has been established, which may add a new dimension to catalyst design by choosing bases with differential basicity. Thus, we believe the current study provides useful chemical information to develop efficient catalysts for CO_2 hydrogenation.

■ ASSOCIATED CONTENT

Supporting Information

Additional computational details, supporting figures, schemes and tables, hydricity calculation details, and Cartesian coordinates of all species involved. The Supporting Information is available free of charge on the ACS Publications website at DOI: 10.1021/acs.inorgchem.5b00469.

■ AUTHOR INFORMATION

Corresponding Author

*E-mail: shengfa.ye@cec.mpg.de.

Notes

The authors declare no competing financial interest.

■ ACKNOWLEDGMENTS

We gratefully acknowledge the financial support from the Max-Planck Society and are thankful to Drs. M. Sparta and D. G. Liakos and Ms. U. Becker for helpful discussions about DLPNO-CCSD(T) calculations. Thanks are due to the learned reviewers who made critical reviews of our manuscript and helped improve its quality.

■ REFERENCES

(1) (a) Arakawa, H.; Aresta, M.; Armor, J. N.; Barteau, M. A.; Beckman, E. J.; Bell, A. T.; Bercaw, J. E.; Creutz, C.; Dinjus, E.; Dixon, D. A.; Domen, K.; DuBois, D. L.; Eckert, J.; Fujita, E.; Gibson, D. H.; Goddard, W. A.; Goodman, D. W.; Keller, J.; Kubas, G. J.; Kung, H. H.; Lyons, J. E.; Manzer, L. E.; Marks, T. J.; Morokuma, K.; Nicholas, K. M.; Periana, R.; Que, L.; Rostrup-Nielson, J.; Sachtler, W. M. H.; Schmidt, L. D.; Sen, A.; Somorjai, G. A.; Stair, P. C.; Stults, B. R.; Tumas, W. *Chem. Rev.* **2001**, *101*, 953−996. (b) Appel, A. M.; Bercaw, J. E.; Bocarsly, A. B.; Dobbek, H.; DuBois, D. L.; Dupuis, M.; Ferry, J. G.; Fujita, E.; Hille, R.; Kenis, P. J. A.; Kerfeld, C. A.; Morris, R. H.; Peden, C. H. F.; Portis, A. R.; Ragsdale, S. W.; Rauchfuss, T. B.; Reek, J. N. H.; Seefeldt, L. C.; Thauer, R. K.; Waldrop, G. L. *Chem. Rev.* **2013**, *113*, 6621−6658. (c) Mondal, B.; Song, J.; Neese, F.; Ye, S. *Curr. Opin. Chem. Biol.* **2015**, *25*, 103−109.

(2) (a) Langanke, J.; Wolf, A.; Hofmann, J.; Böhm, K.; Subhani, M. A.; Müller, T. E.; Leitner, W.; Gürtler, C. *Green Chem.* **2014**, *16*, 1865−1870. (b) Ola, O.; Mercedes Maroto-Valer, M.; Mackintosh, S. *Energy Procedia* **2013**, *37*, 6704−6709.

(3) (a) Jessop, P. G.; Ikariya, T.; Noyori, R. *Chem. Rev.* **1995**, *95*, 259−272. (b) Jessop, P. G.; Joó, F.; Tai, C.-C. *Coord. Chem. Rev.* **2004**, *248*, 2425−2442. (c) Leitner, W. *Angew. Chem., Int. Ed. Engl.* **1995**, *34*, 2207−2221. (d) Federsel, C.; Jackstell, R.; Beller, M. *Angew. Chem., Int. Ed.* **2010**, *49*, 6254−6257. (e) Wang, W.; Wang, S.; Ma, X.; Gong, J. *Chem. Soc. Rev.* **2011**, *40*, 3703−3727.

(4) (a) Leitner, W.; Dinjus, E.; Gassner, F. *J. Organomet. Chem.* **1994**, *475*, 257−266. (b) Tsai, J. C.; Nicholas, K. M. *J. Am. Chem. Soc.* **1992**, *114*, 5117−5124. (c) Gassner, F.; Leitner, W. *J. Chem. Soc., Chem. Commun.* **1993**, 1465−1466. (d) Burgemeister, T.; Kastner, F.; Leitner, W. *Angew. Chem., Int. Ed. Engl.* **1993**, *32*, 739−741.

(5) (a) Tominaga, K.-I.; Sasaki, Y.; Kawai, M.; Watanabe, T.; Saito, M. *J. Chem. Soc., Chem. Commun.* **1993**, 629−631. (b) Wesselbaum, S.; vom Stein, T.; Klankermayer, J.; Leitner, W. *Angew. Chem.* **2012**, *124*, 7617−7620. (c) Tai, C.-C.; Pitts, J.; Linehan, J. C.; Main, A. D.; Munshi, P.; Jessop, P. G. *Inorg. Chem.* **2002**, *41*, 1606−1614. (d) Hayashi, H.; Ogo, S.; Fukuzumi, S. *Chem. Commun.* **2004**, 2714−2715. (e) Getty, A. D.; Tai, C.-C.; Linehan, J. C.; Jessop, P. G.; Olmstead, M. M.; Rheingold, A. L. *Organometallics* **2009**, *28*, 5466−5477. (f) Elek, J.; Nádasdi, L.; Papp, G.; Laurenczy, G.; Joó, F. *Appl. Catal., A* **2003**, *255*, 59−67.

(6) (a) Tanaka, R.; Yamashita, M.; Nozaki, K. *J. Am. Chem. Soc.* **2009**, *131*, 14168−14169. (b) Schmeier, T. J.; Dobereiner, G. E.; Crabtree, R. H.; Hazari, N. *J. Am. Chem. Soc.* **2011**, *133*, 9274−9277. (c) Hull, J. F.; Himeda, Y.; Wang, W.-H.; Hashiguchi, B.; Periana, R.; Szalda, D. J.; Muckerman, J. T.; Fujita, E. *Nat. Chem.* **2012**, *4*, 383−388.

(7) (a) Langer, R.; Diskin-Posner, Y.; Leitus, G.; Shimon, L. J. W.; Ben-David, Y.; Milstein, D. *Angew. Chem., Int. Ed.* **2011**, *50*, 9948−9952. (b) Ziebart, C.; Federsel, C.; Anbarasan, P.; Jackstell, R.; Baumann, W.; Spannenberg, A.; Beller, M. *J. Am. Chem. Soc.* **2012**, *134*, 20701−20704. (c) Jeletic, M. S.; Mock, M. T.; Appel, A. M.; Linehan, J. C. *J. Am. Chem. Soc.* **2013**, *135*, 11533−11536.

(8) (a) Yin, C.; Xu, Z.; Yang, S.-Y.; Ng, S. M.; Wong, K. Y.; Lin, Z.; Lau, C. P. *Organometallics* **2001**, *20*, 1216−1222. (b) Musashi, Y.; Sakaki, S. *J. Am. Chem. Soc.* **2000**, *122*, 3867−3877. (c) Musashi, Y.; Sakaki, S. *J. Am. Chem. Soc.* **2002**, *124*, 7588−7603. (d) Ohnishi, Y.-Y.; Matsunaga, T.; Nakao, Y.; Sato, H.; Sakaki, S. *J. Am. Chem. Soc.* **2005**, *127*, 4021−4032. (e) Ohnishi, Y.-Y.; Nakao, Y.; Sato, H.; Sakaki, S. *Organometallics* **2006**, *25*, 3352−3363. (f) Huff, C. A.; Sanford, M. S. *ACS Catal.* **2013**, *3*, 2412−2416.

(9) Hutschka, F.; Dedieu, A.; Eichberger, M.; Fornika, R.; Leitner, W. *J. Am. Chem. Soc.* **1997**, *119*, 4432−4443.

(10) Tanaka, R.; Yamashita, M.; Chung, L. W.; Morokuma, K.; Nozaki, K. *Organometallics* **2011**, *30*, 6742−6750.

(11) (a) Ahlquist, M. R. S. G. *J. Mol. Catal. A: Chem.* **2010**, *324*, 3−8. (b) Yang, X. *ACS Catal.* **2011**, *1*, 849−854.

(12) Hou, C.; Jiang, J.; Zhang, S.; Wang, G.; Zhang, Z.; Ke, Z.; Zhao, C. *ACS Catal.* **2014**, *4*, 2990−2997.

(13) Ogo, S.; Kabe, R.; Hayashi, H.; Harada, R.; Fukuzumi, S. *Dalton Trans.* **2006**, 4657−4663.

(14) Jeletic, M. S.; Helm, M. L.; Hulley, E. B.; Mock, M. T.; Appel, A. M.; Linehan, J. C. *ACS Catal.* **2014**, *4*, 3755−3762.

(15) (a) Fan, T.; Chen, X.; Lin, Z. *Chem. Commun.* **2012**, *48*, 10808−10828. (b) Yang, X. *Dalton Trans.* **2013**, *42*, 11987−11991. (c) Filonenko, G. A.; Hensen, E. J. M.; Pidko, E. A. *Catal. Sci. Technol.* **2014**, *4*, 3474−3485. (d) Bichler, B.; Holzhacker, C.; Stöger, B.; Puchberger, M.; Veiros, L. F.; Kirchner, K. *Organometallics* **2013**, *32*, 4114−4121.

(16) (a) Harvey, J. N. *Annu. Rep. Prog. Chem., Sect. C: Phys. Chem.* **2006**, *102*, 203−226. (b) Cohen, A. J.; Mori-Sánchez, P.; Yang, W. *Science* **2008**, *321*, 792−794.

(17) Bartlett, R. J.; Musiał, M. *Rev. Mod. Phys.* **2007**, *79*, 291−352.

(18) Řezáč, J.; Hobza, P. *J. Chem. Theory Comput.* **2013**, *9*, 2151−2155.

(19) (a) Riplinger, C.; Neese, F. *J. Chem. Phys.* **2013**, *138*, 034106. (b) Riplinger, C.; Sandhofer, B.; Hansen, A.; Neese, F. *J. Chem. Phys.* **2013**, *139*, 134101.

(20) (a) Sparta, M.; Riplinger, C.; Neese, F. *J. Chem. Theory Comput.* **2014**, *10*, 1099−1108. (b) Sparta, M.; Neese, F. *Chem. Soc. Rev.* **2014**, *43*, 5032−5041.

(21) Neese, F. *WIREs Comput. Mol. Sci.* **2012**, *2*, 73−78.

(22) Zhao, Y.; Truhlar, D. G. *J. Chem. Phys.* **2006**, *125*, 194101.

(23) (a) Pantazis, D. A.; Chen, X.-Y.; Landis, C. R.; Neese, F. *J. Chem. Theory Comput.* **2008**, *4*, 908−919. (b) Schäfer, A.; Horn, H.; Ahlrichs, R. *J. Chem. Phys.* **1992**, *97*, 2571.

DOI: 10.1021/acs.inorgchem.5b00469
Inorg. Chem. 2015, 54, 7192−7198

(24) Schäfer, A.; Huber, C.; Ahlrichs, R. *J. Chem. Phys.* **1994**, *100*, 5829−5835.
(25) Zhao, Y.; Truhlar, D. G. *Acc. Chem. Res.* **2008**, *41*, 157−167.
(26) (a) Becke, A. D. *Phys. Rev. A: At., Mol., Opt. Phys.* **1988**, *38*, 3098−3100. (b) Perdew, J. P.; Wang, Y. *Phys. Rev. B: Condens. Matter Mater. Phys.* **1992**, *45*, 13244−13249.
(27) Grimme, S.; Ehrlich, S.; Goerigk, L. *J. Comput. Chem.* **2011**, *32*, 1456−1465.
(28) (a) Eichkorn, K.; Weigend, F.; Treutler, O.; Ahlrichs, R. *Theor. Chem. Acc.* **1997**, *97*, 119−124. (b) Eichkorn, K.; Treutler, O.; Öhm, H.; Häser, M.; Ahlrichs, R. *Chem. Phys. Lett.* **1995**, *240*, 283−290.
(29) Eichkorn, K.; Treutler, O.; Öhm, H.; Häser, M.; Ahlrichs, R. *Chem. Phys. Lett.* **1995**, *240*, 283−290.
(30) Klamt, A.; Schüürmann, G. *J. Chem. Soc., Perkin Trans. 2* **1993**, 799−805.
(31) (a) Becke, A. D. *Phys. Rev. A: At., Mol., Opt. Phys.* **1988**, *38*, 3098−3100. (b) Becke, A. D. *J. Chem. Phys.* **1993**, *98*, 5648. (c) Lee, C.; Yang, W.; Parr, R. G. *Phys. Rev. B: Condens. Matter Mater. Phys.* **1988**, *37*, 785−789.
(32) Weigend, F.; Köhn, A.; Hättig, C. *J. Chem. Phys.* **2002**, *116*, 3175.
(33) Neese, F.; Wennmohs, F.; Hansen, A.; Becker, U. *Chem. Phys.* **2009**, *356*, 98−109.
(34) Liakos, D. G.; Neese, F. *J. Chem. Theory Comput.* **2011**, *7*, 1511−1523.
(35) (a) Xue, G.; Geng, C.-Y.; Ye, S.; Fiedler, A. T.; Neese, F.; Que, L., Jr. *Inorg. Chem.* **2013**, *52*, 3976−3984. (b) Ye, S.; Riplinger, C.; Hansen, A.; Krebs, C.; Bollinger, M., Jr.; Neese, F. *Chem. - Eur. J.* **2012**, *18*, 6555−6567. (c) Song, J.; Klein, E. L.; Neese, F.; Ye, S. *Inorg. Chem.* **2014**, *53*, 7500−7507. (d) Fang, H.; Jing, H.; Ge, H.; Brothers, P. J.; Fu, X.; Ye, S. *J. Am. Chem. Soc.* **2015**, *137*, 7122−7127.
(36) Connors, K. A. *Chemical Kinetics: The Study of Reaction Rates in Solution*; VCH: New York, 1990; pp 99−101.
(37) Ye, S.; Neese, F. *Inorg. Chem.* **2010**, *49*, 772−774.
(38) (a) Bautista, M. T.; Cappellani, E. P.; Drouin, S. D.; Morris, R. H.; Schweitzer, C. T.; Sella, A.; Zubkowski, J. *J. Am. Chem. Soc.* **1991**, *113*, 4876−4887. (b) Bianchini, C.; Masi, D.; Peruzzini, M.; Casarin, M.; Maccato, C.; Rizzi, G. A. *Inorg. Chem.* **1997**, *36*, 1061−1069.
(39) (a) DuBois, D. L.; Berning, D. E. *Appl. Organomet. Chem.* **2000**, *14*, 860−862. (b) Qi, X.-J.; Fu, Y.; Liu, L.; Guo, Q.-X. *Organometallics* **2007**, *26*, 4197−4203.
(40) (a) Guthrie, J. P. *J. Am. Chem. Soc.* **1996**, *118*, 12886−12890. (b) Evans, M. G.; Polanyi, M. *Trans. Faraday Soc.* **1938**, *34*, 11−23.
(41) (a) Eckert, J.; Albinati, A.; White, R. P.; Bianchini, C.; Peruzzini, M. *Inorg. Chem.* **1992**, *31*, 4241−4244. (b) Ohanessian, G.; Goddard, W. A., III *Acc. Chem. Res.* **1990**, *23*, 386−392.
(42) Muckerman, J. T.; Achord, P.; Creutz, C.; Polyansky, D. E.; Fujita, E. *Proc. Natl. Acad. Sci. U.S.A.* **2012**, *109*, 15657−15662.
(43) Cheng, T.-Y.; Bullock, R. M. *Organometallics* **2002**, *21*, 2325−2331.
(44) Darensbourg, D. J. *Inorg. Chem.* **2010**, *49*, 10765−10780.
(45) Federsel, C.; Ziebart, C.; Jackstell, R.; Baumann, W.; Beller, M. *Chem.—Eur. J.* **2012**, *18*, 72−75.
(46) Badiei, Y. M.; Wang, W.-H.; Hull, J. F.; Szalda, D. J.; Muckerman, J. T.; Himeda, Y.; Fujita, E. *Inorg. Chem.* **2013**, *52*, 12576−12586.
(47) (a) Fontecilla-Camps, J. C.; Volbeda, A.; Cavazza, C.; Nicolet, Y. *Chem. Rev.* **2007**, *107*, 4273−4303. (b) Lubitz, W.; Ogata, H.; Rüdiger, O.; Reijerse, E. *Chem. Rev.* **2014**, *114*, 4081−4148.
(48) Wang, W.-H.; Muckerman, J. T.; Fujita, E.; Himeda, Y. *ACS Catal.* **2013**, *3*, 856−860.

DOI: 10.1021/acs.inorgchem.5b00469
Inorg. Chem. 2015, 54, 7192−7198